Published in final edited form as:
Cell Rep. 2014 November 6; 9(3): 884–892. doi:10.1016/j.celrep.2014.10.001.

Heterochromatin-mediated gene silencing facilitates the diversification of olfactory neurons

David B. Lyons[1], **Angeliki Magklara**[2], **Tracie Goh**[3], **Srihari Sampath**[4,†], **Anne Schaefer**[4,§], **Gunnar Schotta**[5], and **Stavros Lomvardas**[1,3,*,$]

[1]Tetrad Program, University of California, San Francisco, San Francisco, CA 94158, USA

[2]Division of Biomedical Research, Institute of Molecular Biology and Biotechnology, Foundation for Research and Technology-Hellas, Ioannina, Greece

[3]Department of Anatomy, University of California San Francisco, CA 94920, USA

[4]Laboratory of Immune Cell Epigenetics and Signaling, The Rockefeller University, 1230 York Avenue, New York, New York, 10065, USA

[5]Munich Center for Integrated Protein Science, Adolf-Butenandt-Institute, Ludwig Maximilian University, Schillerstrasse 44, 80336 Munich, Germany

SUMMARY

An astounding property of the nervous system is its cellular diversity. This diversity, which was initially realized by morphological and electrophysiological differences, is ultimately produced by variations in gene expression programs. In most cases these variations are determined by external cues. However, a growing number of neuronal types have been identified in which inductive signals cannot explain the few but decisive transcriptional differences that cause cell diversification. Here, we show that heterochromatic silencing, which we find is governed by histone methyltransferases G9a (KMT1C) and GLP (KMT1D), is essential for stochastic and singular OR expression. Deletion of G9a and GLP dramatically reduces the complexity of the OR transcriptome, resulting in transcriptional domination by a few ORs and loss of singularity in OR expression. Thus, in addition to its previously known functions, our data suggest that heterochromatin creates an epigenetic platform that affords stochastic, mutually exclusive gene choices and promotes cellular diversity.

Correspondence regarding this work should be directed to Stavros Lomvardas (sl682@columbia.edu).
†Current address: Genomics Institute of the Novartis Research Foundation, 10675 John Jay Hopkins Drive, San Diego CA 92121 USA.
§Current address: Mount Sinai School of Medicine, One Gustave L. Levy Place, Box 1065, New York, NY 10029 USA.
$Current address: Department of Biochemistry and Molecular Biophysics, Mortimer B. Zuckerman Mind, Brain, and Behavior Institute, Columbia University, New York, NY 10032, sl682@columbia.edu

Author contributions. DBL conceived, designed, and performed experiments, analyzed data, and wrote paper. AM performed ChIP experiments and designed experiments. TG designed experiments and performed FISH and IF. SS, AS, and GS contributed reagents. SL conceived the project, analyzed data, and wrote paper.

INTRODUCTION

Stochastic gene expression is important in generating the diverse cell types of the nervous system. The drosophila Dscam family of alternatively spliced isoforms(Zipursky et al., 2006), photoreceptor choice in mammals and flies(Rister and Desplan, 2011), cellular differentiation within motor neuron pools in the spinal cord(Dasen et al., 2008; Dasen et al., 2005), and the choice of mammalian Protocadherin promoters(Chen and Maniatis, 2013) all provide examples of non-deterministic gene expression programs with critical roles in the generation of neuronal diversity(Chen et al., 2012; Lefebvre et al., 2012). However, the monogenic and monoallelic expression of a single olfactory receptor (OR) gene(Chess et al., 1994) from more than a thousand available alleles (Buck and Axel, 1991) provides the most extreme paradigm of stochastic transcriptional choice that determines the fate, circuitry, and functional identity of an olfactory sensory neuron (OSN).

The molecular mechanisms of OR gene choice in mammals remained unknown until the identification of a feedback signal that stabilizes the expression of the chosen OR allele and prevents the transcriptional activation of additional alleles(Lewcock and Reed, 2004; Serizawa et al., 2003; Shykind et al., 2004). This feedback, which is generated by the OR protein-dependent activation of the ER-resident kinase Perk, leads to transient translation of transcription factor Atf5 and downregulation of histone demethylase Lsd1(Dalton et al., 2013; Lyons et al., 2013). Lsd1 activates OR transcription most likely via the demethylation of lysine 9 of histone H3(Lyons et al., 2013), an epigenetic mark that is deposited on OR genes at the early stages of OSN differentiation, along with histone H4 lysine 20 trimethylation (Magklara et al., 2011).

These observations suggest that the heterochromatic silencing of OR genes plays an important role in singular and stochastic OR expression. First, it keeps the non-chosen ORs completely silent, thereby ensuring coherent neuronal targeting and activity. Second, it affords a feedback process, which “silences the de-silencer” and, thus, prevents activation of additional ORs without affecting the expression of the already chosen allele. It is not clear from these data, however, whether H3K9 demethylation, ostensibly required based on the effects of Lsd1 deletion, is also sufficient for OR transcription. In other words, it remains unknown if the stochastic H3K9 demethylation of a single allele constitutes the singular choice *per se*, or an additional superimposed mechanism provides the initial singularity of choice. Because perturbations in the OR-elicited feedback result in frequent OR switching but not simultaneous co-expression of multiple OR alleles (Dalton et al., 2013; Lyons et al., 2013), the latter hypothesis is more likely. However, recent theoretical models suggest that singular OR expression could also be explained just by a combination of a slow H3K9 demethylation process and a fast feedback that blocks further demethylation(Tan et al., 2013). In this scenario, removal of the repressive histone marks from a randomly chosen OR allele could be essential and sufficient for OR expression, a hypothesis supported by pharmacological inhibition of G9a/GLP in zebrafish embryos(Ferreira et al., 2014).

Here, we genetically remove both H3K9 (G9a and GLP) and H4K20 (SUV4–20H1 and –H2) histone methyltransferases, which we find are responsible for repressive lysine methylation at OR genes. In the case of H3K9me3 disruption, OR expression becomes

heavily skewed toward a small subset of OR genes at the expense of all other ORs, such that the MOE becomes reproducibly homogenous. These few, dominating ORs defy the "one receptor per neuron" rule, but at low frequency. Furthermore, we find that the severe skew toward these OR genes is G9a/Glp-dose dependent. In contrast, we eliminated H4K20me3 and found no overt phenotype at the level of OR expression. Together, these data link H3K9me3-based heterochromatic OR gene silencing to the diversity of OR expression and the broad chemical sensitivity of the mammalian nose.

RESULTS

Removal of G9a and GLP severely deregulates OR expression

To test how removal of repressive heterochromatic histone marks affects OR choice, we deleted H3K9 and H4K20 methyltransferases from the developing main olfactory epithelium (MOE). Because OR loci are first marked with H3K9me2, and only upon further differentiation with H3K9me3 and H4K20me3 (Magklara et al., 2011), we reasoned that H3K9me2 is the substrate upon which OR chromatin is further methylated in the OSN lineage. In this scenario prevention of H3K9 di-methylation early would also prevent subsequent tri-methylation, resulting in OR chromatin devoid of repressive H3K9 methylation. To remove H3K9me2 activity before the addition of the extra methyl-group on H3K9, we crossed G9a(Tachibana et al., 2005) and GLP floxed alleles (Schaefer et al., 2009) to Foxg1-Cre that is expressed very early, during olfactory placode development (Hébert and McConnell, 2000). Because the KO mice die perinatally, our analysis was restricted to the last day of gestation (embryonic day 18.5).

For a global view of the transcriptional consequences of G9a and GLP deletion, we performed RNA-seq analysis in G9a/GLP double knockouts (dKO). Surprisingly, genomewide transcription is not heavily affected by homozygote deletion of G9a and GLP together—the number of genes that increase or decrease beyond a $\log_2$ fold-change of 2 is limited to a small fraction of the total transcriptome (66 of 19,850 Ensembl gene records included in this analysis, only three of which are known transcriptional regulators; Figure 1B and Table S1). In contrast, OR expression is profoundly misregulated by loss of G9a and GLP, with a few OR genes being markedly upregulated and most OR genes being downregulated (Figure 1A). One OR in particular, Olfr231, is upregulated by ~90-fold in the double KO MOEs, a result confirmed by RNA FISH (Figure 1C). Strikingly, Olfr231$^+$ OSNs fill the entire MOE, abandoning the zonal pattern of expression typically seen for OR genes (Figure S1A).

G9a/GLP deletion disrupts the "one receptor per neuron" rule

The high cellular frequency of Olfr231 expression in the G9a/GLP dKO MOEs suggests that the singularity of OR expression may be perturbed in the mutant mice, since other ORs are also expressed with increased frequency. To test this directly, we performed 2 color FISH with Cy3-labeled Olfr231 (red) and a pool of probes against the next-most highly expressed OR genes, labeled with fluorescein (green; Olfr878 pool, Fig. 2A). Remarkably, although we never see coexpression in control sections, we found that Olfr231 is coexpressed in low frequency with at least one of the other ORs in sections from the dKO MOEs (Figure 2B–

C). This is a profound violation of the "one receptor per neuron rule." Despite this, double KO OSNs express mature OSN markers at nearly wild type levels, and their axons reach the olfactory bulb (Figure S2H). Furthermore, double KO OSNs, likely retain their ability to elicit an OR-dependent feedback, since Atf5 translation, as well as LSD1 and Adcy3 expression appear indistinguishable between control and double KO MOEs (Figure S3F–G). This observation suggests that OR clusters are devoid of H3K9 methylation in the G9a/GLP dKO, rendering dynamic Lsd1 activity insufficient for singular OR expression.

G9a/GLP govern the formation of OR heterochromatin

To test the effects of G9a/GLP deletion in the heterochromatinization of OR loci we used imaging-based approaches, since ChIP-based assays are not feasible with the limited number of olfactory neurons in embryonic MOEs and the infrequency by which we obtain double conditional KO mice. OR genes physically cluster together in a few topological clusters in the nucleus that are enriched for H3K9me3 and are functionally important for the singular expression of ORs (Clowney et al., 2012). We thus performed DNA FISH with a complex probe that recognizes the majority of OR genomic clusters in the genome ("pan-OR") and immunofluorescence (IF) with an antibody against H3K9me3, as previously described (Clowney et al., 2012). Pan-OR DNA FISH shows that OR aggregation still occurs in the G9a/Glp double KO (Figure 3A–B). However, we observe statistically significant differences in the organization of the OR foci. Quantitation of the radial distribution of signal intensity in the OR foci shows that the average radius of these foci increases from 12 pixels in control nuclei to 17 pixels in nuclei from the dKO sections (Figure 3C, top; n=100, $p < 0.001$, Student's unpaired t-test). This increase may reflect de-compaction of the OR chromatin in the double KO. Moreover, there is a highly significant increase in the signal intensity of the pan-OR probe outside the OR foci in the dKO nuclei (Figure 3C, bottom, $p < 0.001$), which could also reflect increased accessibility of the pan-OR probe or incomplete nuclear aggregation of the OR loci.

In contrast to the small effects in the nuclear organization of the OR loci, we detect an overt decrease of H3K9me3 at the OR foci in the double KO nuclei (compare Fig 3E–F to G–H; Pearson's (r) and Manders' coefficients (M), $r_{control}=0.657$; $r_{dKO}=0.275$; $M_{control}=0.882$; $M_{dKO}=0.361$). Importantly, in the double KO, overall levels of H3K9me3 in the heterochromatic chromocenters remain high (Figure 3D), which is expected because G9a/Glp do not play a significant role in the trimethylation of pericentromeric and subtelomeric repeats (Shinkai and Tachibana, 2011); instead trimethylation of pericentromeric and subtelomeric repeats is accomplished by Suv39H1 and −H2 (Schotta et al., 2004), which tri-methylate H3K9 in these genomic loci much prior to the deletion of G9a/Glp by Foxg1-Cre. Therefore, G9a/GLP deletion from the differentiating MOE reduces the levels of H3K9me3 from OR loci and affects the nuclear organization of OR loci. This observation is consistent with recent experiments demonstrating a direct correlation between epigenetic state and nuclear distribution in mammalian cells (Pinheiro et al., 2012). However it should be noted that the overall aggregation of OR genes still takes place in the dKO nuclei, in sharp contrast with the complete disruption of these structures upon ectopic Lamin-B receptor (Lbr) expression in mOSNs (Clowney et al., 2012)

H4K20me3 has non-essential function in OR gene repression

To examine whether trimethylation of H4K20 is as important in OR gene regulation as trimethylation of H3K9, we generated conditional dKO mice by crossing Foxg1-Cre and Suv4–20H1 floxed allele (Schotta et al., 2004) to the Suv4–20H2 KO allele. Because these mice are viable, we analyzed the dKO postnatally so we could biochemically address the effect of the deletion in H4K20 trimethylation. Although our ChIP-qPCR analysis shows that in dKO MOEs H4K20me3 is significantly reduced at OR genes (Figure S3E), our RNA-seq, qRT-PCR, and IF analysis shows that OR expression is not affected by loss of this histone modification (Figure S3A,C–D). Both the mean and median levels of OR expression remain the same between control and double KO MOEs (Figure S3A), the number of OR alleles detected is nearly identical (ORs detected in dHet: 1019; ORs detected in dKO: 1020). In agreement with a more dominant role in OR gene expression, H3K9me3 levels remain high on OR loci in the double KO, consistent with previous observations (Schotta et al., 2004) that dissociate H3K9 from H4K20 methylation (Figure S3A).

LSD1 is partially dispensable in the setting of reduced H3K9 methylation

Since Olfr231 is expressed at a significantly higher frequency in the G9a/GLP dKO, we hypothesized that its expression is independent of Lsd1-mediated H3K9 demethylation. If this were true, then deletion of Lsd1 should have no impact on Olfr231 expression in the G9a/GLP dKO background. Because generation of a conditional triple KO was not feasible, we asked if single deletion of G9a or GLP results in increased Olfr231 expression frequency as seen in G9a/GLP dKO. Indeed, RNA-seq, qRT-PCR, and RNA-FISH analysis in either G9a or GLP single KO reveals a significant increase in the number of Olfr231 expressing neurons, suggesting that the two methyltransferases are partially redundant in the MOE (Figure 4A and Figure S4A–B). This allowed us to test whether Lsd1 is required in the G9a KO setting for the increase in Olfr231. Although Olfr231 expression is completely abolished in the Lsd1 KO MOEs (Figure 4A) its expression is partially restored in the G9a/Lsd1 dKO MOEs, supporting direct and opposing roles of the two enzymes in H3K9 methylation of OR loci. The fact that G9a deletion in the Lsd1 KO background does not restore Olfr231 expression to the levels of the G9a single KO is likely explained by compound toxicity of the two independent deletions. Additionally, we reasoned that if there were a reduced role for LSD1 in the activation of ORs in the G9a KO MOE, a comparison of the DNA damage produced by its activity, 8-oxoguanosine, would reflect this LSD1 independence (Lyons et al. 2013). Indeed, we find no evidence for increased LSD1 activity at the Olfr231 locus in the G9a single KO compared to the control 8-oxoguanosine DNA immunoprecipitation (Figure 4B). These observations support a model where G9a and GLP methylate H3K9 on every OR gene and then Lsd1 stochastically demethylates H3K9 from the chosen OR allele. In agreement with a sequential fashion by which H3K9 methylation and demethylation regulate OR expression, deletion of G9a immediately after OR choice, or upon terminal neuronal differentiation have no detectable consequences in OR expression or axonal targeting (Figure S1B–D).

G9a and GLP drive the diversification of OR expression in a dose dependent fashion

The observation that G9a KO has an intermediate OR expression phenotype compared to the G9a/GLP dKO is intriguing. Since both genes are very likely to be coexpressed in the same cells of the MOE (Figure S4C), an explanation for this phenotype is that OR silencing is effective only in the presence of both enzymes. We previously showed that OR heterochromatin forms blocks that extend throughout their genomic clusters (Magklara et al., 2011), thus, it is possible that high concentration of these enzymes is required for the complete marking of the OR chromatin, and that by reducing the number of functional methyltransferase alleles, H3K9 methylation at OR loci becomes incomplete. To test this, we performed RNA-seq on G9a KO as well as G9a KO; GLP heterozygote MOEs to compare with the double KO and control samples. Strikingly, we observe a direct dose-dependency for G9a/GLP levels on OR expression. Olfr231, and the rest of the ORs that are upregulated in the dKO, increase their expression as the number of methyltransferase alleles decreases (Figure 4C). Interestingly, at the same time the number of detected ORs decreases stepwise with each additional missing G9a/GLP allele as fewer ORs contribute to OSN diversity (Figure S2A and Figure 4C). Mean OR transcription remains similar across samples (mean RPKM=0.37; s.d.=0.14) but median OR RPKM is severely reduced in MOE lacking these methyltransferases (Figure S2B), indicating a reduction in the complexity of the transcribed OR repertoire. The complexity of the OR transcriptome can be best depicted with a Lorenz curve, which was first used for the description of income inequality among nations (Lorenz, 1905). In this graph, which shows cumulative OR expression levels, each OR gene contributes a percentage of total expression; the more equally each OR contributes to the total expression, the lower the Gini coefficient is. Thus, if each OR gene had equal contribution to the cumulative OR transcriptome, the Lorenz curve would approach the diagonal of perfect equality, and Gini coefficient would be zero (Figure 4D and Figure S2C–D)(Wittebolle et al., 2009). In control mice, 85% of the ORs contribute to the total OR mRNA and the Lorenz curve is the closest to the diagonal. In contrast, in the dKO, less than 20% of the OR genes account for all of the observed OR gene expression, providing the highest deviation from the perfect diagonal (Figure 4D). The rest of the genotypes examined have intermediate levels of OR diversity that decreases with the number of available mehtyltransferase alleles (Figure 4D). Importantly, the decreased equality of OR expression in the dKO is counterbalanced by dramatically increased transcription of fewer than 10 OR genes, which correspond to 6.4% of the total OR transcriptome in control MOEs and 60% in the double KO (Figure 4C). In contrast, the complexity of the OR transcriptome remains the same in the Suv4–20h1/h2 dKO MOEs (Figure S3B).

DISCUSSION

The data presented here demonstrate that OR heterochromatinization is critical for proper OR expression. In the double G9a/GLP KO MOEs, where H3K9me3 is significantly reduced from the OR genome, the vast majority of ORs are not highly transcribed at the cellular level, whereas fewer than 10 ORs are expressed in most OSNs. In addition to their zonal expansion, these ORs evade the “one receptor per neuron” rule according to our two color RNA FISH experiments. Remarkably, although OR gene silencing is significantly reduced in the G9a/GLP KO MOEs, coexpression among the 10 dominant ORs is infrequent

(Figure 2). Thus, for most ORs, H3K9 demethylation is necessary but not sufficient for expression at high cellular levels. Although recent theoretical calculations support that a slow demethylation process combined with a fast feedback can explain singular OR expression (Tan et al., 2013), our experimental findings suggest that an additional regulatory layer may also contribute to the singularity of OR choice. Were the absence of H3K9 methylation sufficient for robust OR transcription, then most G9a/GLP KO OSNs should express multiple ORs at high levels. Instead, we observe only a subset of OR genes being expressed at high levels throughout the MOE and only occasional coexpression of more than one OR per sensory neuron (Figure 2).

In this note, our data, with the exemption of the few upregulated ORs, diverge from recent observations in zebrafish OSNs, whereby pharmacological inhibition of G9a/Glp results in increased frequency of OR co-expression (Ferreira et al., 2014). Although in zebrafish embryos the global effects of G9a/Glp inhibition on OR transcription were not determined, inhibition of G9a/Glp caused robust OR co-expression for several ORs analyzed by two-color RNA FISH, suggesting that de-silencing is sufficient for robust OR expression in this organism. Thus, despite the deep conservation of H3K9 methylation in OR regulation from fish to mammals, the lineage leading to mice has gained what could be termed a “singularity enforcer” that adds a regulatory layer to OR choice. The source of this singularity may be the stochastic convergence of multiple distant enhancer elements in a unique nuclear location of the olfactory neurons (Markenscoff-Papadimitriou et al., Cell in press). This additional layer may be helping to ensure singular expression in the face of logarithmic expansion of this gene family in terrestrial vertebrates compared to fish (Nei et al., 2008). Obviously, we cannot excluded the intriguing possibility that G9a/Glp, beyond their H3K9 methyltransferase activity, have additional regulatory functions that are not perturbed by pharmacological inhibition but are only revealed upon genetic deletion of the whole protein.

It is possible that both loss of H3K9me3 and complete disruption of the OR aggregates, like the one caused by ectopic Lbr expression in mature OSNs (Clowney et al., 2012), are required for robust expression from multiple ORs. Moreover, although loss of H4K20me3 from OR clusters does not have detectable transcriptional consequences, the removal of this mark may also be essential for robust OR expression, explaining why loss of H3K9 methylation does not cause frequent OR coexpression. Both scenarios are not currently testable since they require crossing several additional alleles to the G9a/Glp double KO. Moreover, we cannot exclude that indirect effects from these genetic manipulations convolute the interpretation of our analysis. However, our previous work showed that in OSNs H3K9me3 is deposited almost exclusively on OR genes and pericentromeric and subtelomeric repeats (Magklara et al., 2011). In agreement with this, our RNAseq data from G9a/Glp KO mice suggest that by-and-large only OR genes are significantly affected by this deletion. Finally, the fact that mature OSN markers and components of the OR feedback signal have normal expression levels and distribution (Figure S2E–H), make the possibility of indirect effects less likely.

Our findings pose an important question: why in the absence of heterochromatic silencing are only these few ORs expressed at significant cellular levels? We propose that chromatin mediated silencing, which occurs before the onset of OR transcription, masks the DNA

sequence of OR promoters and equalizes their frequency of choice, explaining the relatively equal representation of ORs observed in control MOEs. According to this model, Lsd1 and the rest of the OR transcriptional machinery cannot "predict" *a priori* the strength of an OR promoter, making the exact sequence of the promoter irrelevant for the initial choice. In the G9a/GLP dKO with much reduced H3K9 methylation, the role for Lsd1-mediated activation is accordingly diminished, and stronger OR promoters may prevail, transforming a stochastic process to a deterministic one. Computational analysis comparing the promoters of the most upregulated ORs with the rest of the repertoire failed to reveal significant differences in predicted transcription factor binding motifs (data not shown). Moreover, de novo motif analysis revealed only differences in low complexity repetitive sequences, for which there are no data supporting a role in transcriptional activation (data not shown). Thus, at the moment, the reason(s) why certain ORs are specifically upregulated in a reproducible manner across multiple experimental animals remains mysterious, and likely will remain so until we obtain a comprehensive understanding of the transcription factors that bind to and regulate OR transcription.

Importantly, whatever transcription factors are responsible for the increased expression frequencies of Olfr231 and the other upregulated ORs, they are not expressed in a zonal fashion, since in the double KO zonal boundaries are violated (Figure S1A). This could in fact provide mechanistic insight into the zonal nature of OR expression, which may not be primarily determined by zonal expression of specific transcription factors, but by the selective de-methylation of specific OR clusters within different zones, in agreement with the homogeneity among OR promoters from different zones(Clowney et al., 2011).

In summary, for OR genes, heterochromatinization facilitates their singular, stochastic selection, ascribing a novel regulatory role for heterochromatic gene silencing as that of a source of cellular diversity. Interestingly, it was recently reported that silencing, in this case in the form DNA methylation by Dnmt3b, also governs the stochastic and mutually exclusive nature of clustered protocadherin gene expression(Toyoda et al., 2014). With an increasing number of reports of widespread stochastic and monoallelic expression during mammalian development (Deng et al. 2014; Eckersley-Maslin et al., 2014; Nag et al., 2013) it will be interesting to examine whether epigenetic silencing is generally used for the diversification of gene expression programs.

EXPERIMENTAL PROCEDURES

Animals

All mice were housed in standard conditions with a 12-hour light/dark cycle and access to food and water ad libitum and in accordance with the University of California IACUC guidelines. All strains were maintained on a mixed genetic background. Mouse strains used are as follows: Foxg1-Cre(Hebert and McConnell, 2000), OMP-IRES-Cre(Eggan et al., 2004), MOR28-IRES-Cre(Shykind et al., 2004), R26R mT/mG (Muzumdar et al., 2007), G9a flox(Tachibana et al., 2005), GLP flox(Schaefer et al., 2009), Lsd1 flox(Wang et al., 2007), SUV4–20H1 flox and SUV4–20H2 null(Schotta et al., 2004).

DNA Deep Sequencing

Sequencing was performed on the Illumina HiSeq 2000 and −2500. cDNA libraries for all samples were prepared with the ScriptSeq kit V2 (Epicentre, Illumina) with total mappable reads from 50-bp paired end reads as follows: G9a heterozygote: 69,620,496; G9a KO: 73,023,480; G9a KO/GLP heterozygote: 67,119,073; G9a/GLP double KO: 59,623,472; SUV4–20H1/H2 double heterozygote: 52,438,433; SUV4–20 double knockout: 46,703,558. Sequencing files are available on the GEO database under accession number GSE54473.

Sequence Data analysis

RNA-seq reads were mapped with Tophat (Trapnell et al., 2009) using Bowtie (Langmead et al., 2009). Differential expression was quantified with the Cufflinks software package (Trapnell et al., 2010) using classic-fpkm library normailization methods. Downstream visualization was carried out with a combination of Excel (Microsoft) and R (http://www.R-project.org.). Lorenz curves were generated with the Ineq R package (http://cran.r-project.org/web/packages/ineq/) and additional visualization of RNA-seq data was carried out in Perl using Circos data visualization software (Krzywinski et al., 2009).

In situ hybridization

16 μm cryosections were air-dried briefly at 37°C before 10 minute fixation in ice-cold 4% paraformaldehyde in phosphate-buffered saline (PBS) at pH 7.4. PBS with 0.1% Tween was used to wash the slides thrice prior to one 10 minute acetylation step carried out in DEPC-treated water. A single PBS-Tween wash immediately preceded the pre-hybridization step, in which slides are submerged in a room-temperature solution containing 50% formamide, 5X SSC, Denhardt's solution, and yeast tRNA. Probes were diluted in this solution and hybridized to sections overnight at 65°C after which slides were washed briefly in 65°C 5X SSC then for 90 minutes in 0.2X SSC again at 65°C. 0.1M Tris-HCl / 0.15M NaCl buffer at pH 7.5 was then used to wash slides, followed by a 1-hr blocking step in 10% sheep serum in Tris/NaCl. Slides were then incubated overnight at 4°C in 1% sheep serum with anti-digoxigenin conjugated alkaline phosphatase (Roche). Tris pH 9.5 buffer with 1mM levamisole and 0.3% Tween-20 was used as the buffer for the NBT/BCIP (Roche) color reaction.

Fluorescent ISH was carried out similarly, with the following differences: following the initial 0.1M Tris-HCl washes after hybridization, 0.5% block (Perkin Elmer) in Tris buffer was applied to the slides for 30 minutes followed by an anti-digoxigenin antibody conjugated to peroxidase (Roche) incubation in TNB at 1:500 for 30 minutes. ISH was developed using TSA reagent (Perkin-Elmer).

For 2 color ISH, both probes were detected using TSA signal amplification (Perkin Elmer) with a 30% hydrogen peroxide wash between development steps to quench peroxidase.

DNA FISH/Immunofluoresence

IF for H3K9me3 (abcam 8898) was performed as described above, prior to annealing DNA FISH probes. "pan-OR" DNA probe was synthesized as previously described(Clowney et al., 2012). Following the addition of Alexa-conjugated secondary AB, sections were fixed

for 10 minutes in 2–4mM EGS at 37 degrees C. DNA FISH was performed using standard protocol. Briefly, RNAse1 treatment was carried out at 37 deg. C. for 1 hr followed by 0.1N HCl treatment. Probes were applied following brief denaturation at exactly 85 degrees C in 75% formamide in 2X SSC. Probes were detected with Dylight 488-conjugated anti-biotin (Jackson ImmunoResearch) following 8% formamide in PT washes.

DNA Immunoprecipitation

Purified genomic DNA was sonicated in PBS with 0.5% Tween-20 to approximately 400-bp fragments using the Bioruptor (Diagenode). For sorted cells, fragmentation of DNA was assumed to be complete following 15 minutes of sonication using medium power output with samples on ice. 8-oxodG monoclonal antibody (Trevigen) was incubated with DNA rotating overnight at 4°C prior to immunoprecipitation.

Microscopy and image analysis

All images were captured with a Zeiss LSM 700 confocal microscope. Pixel intensity scatterplots from Zen stock software of entire image planes were directly exported to Adobe Photoshop to increase blue signal intensity (these points lacked sufficient contrast in raw image); single cross-section intensity tables were exported and plotted using R. The JACoP plugin for ImageJ was used for the generation of both Pearson's correlation and Manders' coefficients in association with data in Figure 3; image intenstiy calculation and quantitation of pan-OR signal distribution was done with the Radial Profile plugin.

Supplementary Material

Refer to Web version on PubMed Central for supplementary material.

Acknowledgments

We would like to thank Drs. Yoichi Shinkai and Makoto Tachibana for kindly sharing their G9a floxed mouse, as well as Dr. Alexander Tarakhovsky for his help in procuring the GLP floxed allele. We would like to thank Drs. Richard Axel and Tom Maniatis as well as members of the Lomvardas lab for critical reading of the manuscript. Work in the lab of SL was funded by the Roadmap for Epigenomics grant R01DA030320, EUREKA grant 5R01MH091661, and the Mcknight Foundation. Work in the lab of GS was funded by grants from the Deutsche Forschungsgemeinschaft (SFB1064, SPP1356, SFB684).

References

Buck L, Axel R. A novel multigene family may encode odorant receptors: a molecular basis for odor recognition. Cell. 1991; 65:175–187. [PubMed: 1840504]

Chen WV, Alvarez FJ, Lefebvre JL, Friedman B, Nwakeze C, Geiman E, Smith C, Thu CA, Tapia JC, Tasic B, et al. Functional significance of isoform diversification in the protocadherin gamma gene cluster. Neuron. 2012; 75:402–409. [PubMed: 22884324]

Chen WV, Maniatis T. Clustered protocadherins. Development (Cambridge, England). 2013; 140:3297–3302.

Chess A, Simon I, Cedar H, Axel R. Allelic inactivation regulates olfactory receptor gene expression. Cell. 1994; 78:823–834. [PubMed: 8087849]

Clowney EJ, Legros MA, Mosley CP, Clowney FG, Markenskoff-Papadimitriou EC, Myllys M, Barnea G, Larabell CA, Lomvardas S. Nuclear aggregation of olfactory receptor genes governs their monogenic expression. Cell. 2012; 151:724–737. [PubMed: 23141535]

Clowney EJ, Magklara A, Colquitt BM, Pathak N, Lane RP, Lomvardas S. High-throughput mapping of the promoters of the mouse olfactory receptor genes reveals a new type of mammalian promoter and provides insight into olfactory receptor gene regulation. Genome research. 2011; 21:1249–1259. [PubMed: 21705439]

Dalton RP, Lyons DB, Lomvardas S. Co-opting the unfolded protein response to elicit olfactory receptor feedback. Cell. 2013; 155:321–332. [PubMed: 24120133]

Dasen JS, De Camilli A, Wang B, Tucker PW, Jessell TM. Hox repertoires for motor neuron diversity and connectivity gated by a single accessory factor, FoxP1. Cell. 2008; 134:304–316. [PubMed: 18662545]

Dasen JS, Tice BC, Brenner-Morton S, Jessell TM. A Hox regulatory network establishes motor neuron pool identity and target-muscle connectivity. Cell. 2005; 123:477–491. [PubMed: 16269338]

Eggan K, Baldwin K, Tackett M, Osborne J, Gogos J, Chess A, Axel R, Jaenisch R. Mice cloned from olfactory sensory neurons. Nature. 2004; 428:44–49. [PubMed: 14990966]

Ferreira T, Wilson SR, Choi YG, Risso D, Dudoit S, Speed TP, Ngai J. Silencing of Odorant Receptor Genes by G Protein betagamma Signaling Ensures the Expression of One Odorant Receptor per Olfactory Sensory Neuron. Neuron. 2014; 81:847–859. [PubMed: 24559675]

Hebert JM, McConnell SK. Targeting of cre to the Foxg1 (BF-1) locus mediates loxP recombination in the telencephalon and other developing head structures. Developmental biology. 2000; 222:296–306. [PubMed: 10837119]

Krzywinski M, Schein J, Birol I, Connors J, Gascoyne R, Horsman D, Jones SJ, Marra MA. Circos: an information aesthetic for comparative genomics. Genome research. 2009; 19:1639–1645. [PubMed: 19541911]

Langmead B, Trapnell C, Pop M, Salzberg SL. Ultrafast and memory-efficient alignment of short DNA sequences to the human genome. Genome Biol. 2009; 10:R25. [PubMed: 19261174]

Lefebvre JL, Kostadinov D, Chen WV, Maniatis T, Sanes JR. Protocadherins mediate dendritic self-avoidance in the mammalian nervous system. Nature. 2012; 488:517–521. [PubMed: 22842903]

Lewcock JW, Reed RR. A feedback mechanism regulates monoallelic odorant receptor expression. Proceedings of the National Academy of Sciences of the United States of America. 2004; 101:1069–1074. [PubMed: 14732684]

Lyons DB, Allen WE, Goh T, Tsai L, Barnea G, Lomvardas S. An epigenetic trap stabilizes singular olfactory receptor expression. Cell. 2013; 154:325–336. [PubMed: 23870122]

Magklara A, Yen A, Colquitt BM, Clowney EJ, Allen W, Markenscoff-Papadimitriou E, Evans ZA, Kheradpour P, Mountoufaris G, Carey C, et al. An epigenetic signature for monoallelic olfactory receptor expression. Cell. 2011; 145:555–570. [PubMed: 21529909]

Muzumdar MD, Tasic B, Miyamichi K, Li L, Luo L. A global double-fluorescent Cre reporter mouse. Genesis. 2007; 45:593–605. [PubMed: 17868096]

Nei M, Niimura Y, Nozawa M. The evolution of animal chemosensory receptor gene repertoires: roles of chance and necessity. Nature reviews. 2008; 9:951–963.

Pinheiro I, Margueron R, Shukeir N, Eisold M, Fritzsch C, Richter FM, Mittler G, Genoud C, Goyama S, Kurokawa M, et al. Prdm3 and Prdm16 are H3K9me1 methyltransferases required for mammalian heterochromatin integrity. Cell. 2012; 150:948–960. [PubMed: 22939622]

Rister J, Desplan C. The retinal mosaics of opsin expression in invertebrates and vertebrates. Developmental neurobiology. 2011; 71:1212–1226. [PubMed: 21557510]

Schaefer A, Sampath SC, Intrator A, Min A, Gertler TS, Surmeier DJ, Tarakhovsky A, Greengard P. Control of cognition and adaptive behavior by the GLP/G9a epigenetic suppressor complex. Neuron. 2009; 64:678–691. [PubMed: 20005824]

Schotta G, Lachner M, Sarma K, Ebert A, Sengupta R, Reuter G, Reinberg D, Jenuwein T. A silencing pathway to induce H3-K9 and H4-K20 trimethylation at constitutive heterochromatin. Genes & development. 2004; 18:1251–1262. [PubMed: 15145825]

Serizawa S, Miyamichi K, Nakatani H, Suzuki M, Saito M, Yoshihara Y, Sakano H. Negative feedback regulation ensures the one receptor-one olfactory neuron rule in mouse. Science (New York, NY. 2003; 302:2088–2094.

Shinkai Y, Tachibana M. H3K9 methyltransferase G9a and the related molecule GLP. Genes & development. 2011; 25:781–788. [PubMed: 21498567]

Shykind BM, Rohani SC, O'Donnell S, Nemes A, Mendelsohn M, Sun Y, Axel R, Barnea G. Gene switching and the stability of odorant receptor gene choice. Cell. 2004; 117:801–815. [PubMed: 15186780]

Tachibana M, Ueda J, Fukuda M, Takeda N, Ohta T, Iwanari H, Sakihama T, Kodama T, Hamakubo T, Shinkai Y. Histone methyltransferases G9a and GLP form heteromeric complexes and are both crucial for methylation of euchromatin at H3-K9. Genes & development. 2005; 19:815–826. [PubMed: 15774718]

Tan L, Zong C, Xie XS. Rare event of histone demethylation can initiate singular gene expression of olfactory receptors. Proceedings of the National Academy of Sciences of the United States of America. 2013; 110:21148–21152. [PubMed: 24344257]

Toyoda S, Kawaguchi M, Kobayashi T, Tarusawa E, Toyama T, Okano M, Oda M, Nakauchi H, Yoshimura Y, Sanbo M, et al. Developmental epigenetic modification regulates stochastic expression of clustered protocadherin genes, generating single neuron diversity. Neuron. 2014; 82:94–108. [PubMed: 24698270]

Trapnell C, Pachter L, Salzberg SL. TopHat: discovering splice junctions with RNA-Seq. Bioinformatics. 2009; 25:1105–1111. [PubMed: 19289445]

Trapnell C, Williams BA, Pertea G, Mortazavi A, Kwan G, van Baren MJ, Salzberg SL, Wold BJ, Pachter L. Transcript assembly and quantification by RNA-Seq reveals unannotated transcripts and isoform switching during cell differentiation. Nat Biotechnol. 2010; 28:511–515. [PubMed: 20436464]

Wang J, Scully K, Zhu X, Cai L, Zhang J, Prefontaine GG, Krones A, Ohgi KA, Zhu P, Garcia-Bassets I, et al. Opposing LSD1 complexes function in developmental gene activation and repression programmes. Nature. 2007; 446:882–887. [PubMed: 17392792]

Zipursky SL, Wojtowicz WM, Hattori D. Got diversity? Wiring the fly brain with Dscam. Trends in biochemical sciences. 2006; 31:581–588. [PubMed: 16919957]

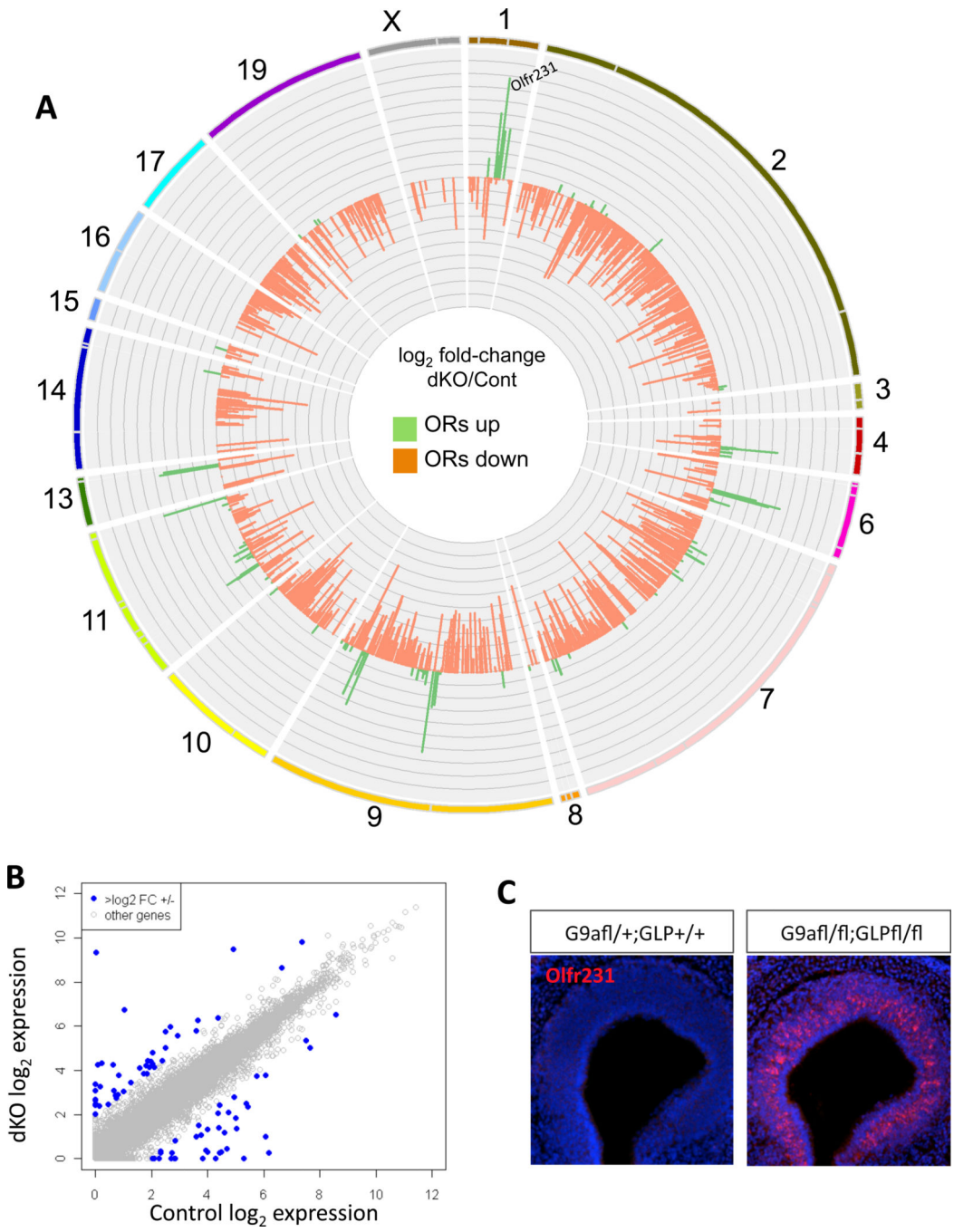

Figure 1. H3K9 methyltransferases G9a and GLP are needed for OR expression and ensure neuronal diversity in the MOE

(**A**) Circos plot(Krzywinski et al., 2009) depicting fold change in all olfactory receptor (OR) genes calculated as $\log_2$ of G9a/GLP double knockout (dKO) (OR RPKM + 1) / G9a heterozygote (OR RPKM +1). Chromosomes are shown as an ideogram with differently colored lines. Each OR cluster is delineated by a grey line dividing the chromosome ideogram such that the relative size of each cluster is maintained. Position of Olfr231 is denoted on Chr.1. y-axis ranges from −7 to 7. Axis marks are every 0.7. (**B**) Non-

chemoreceptor genes were plotted as a function of their expression levels in control and dKO. Genes up- or downregulated $\log_2$ 2-fold or more are shown in blue and are listed in Table S1. (**C**) RNA fluorescent in situ hybridization (FISH) of Olfr231 in Cre-negative control MOEs (left) and G9a-GLP dKO (right). DAPI nuclear stain shown in blue.

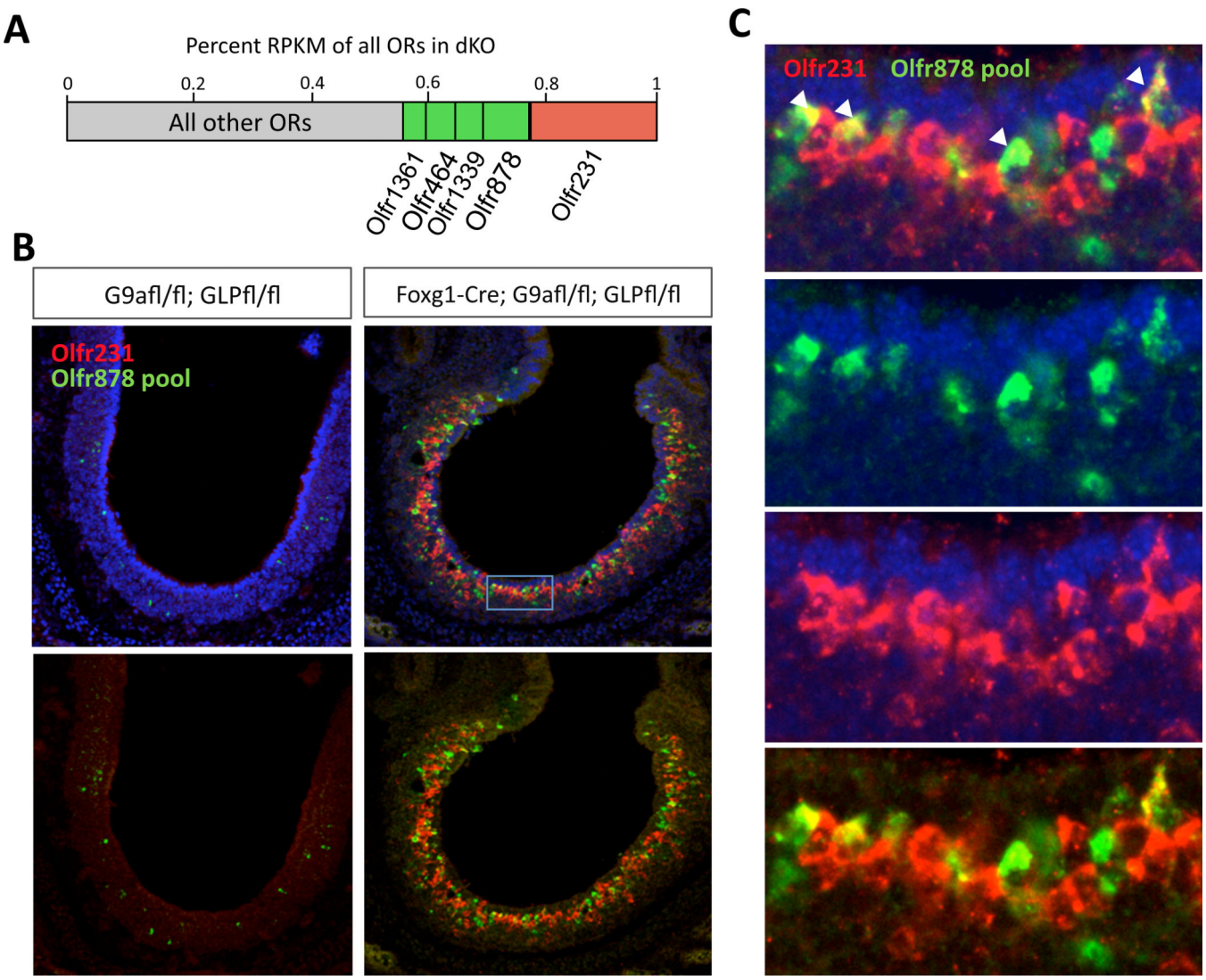

Figure 2. Coexpression of multiple ORs in OSNs lacking G9a and GLP

(A) Barplot illustrating relative expression level of 5 most highly expressed ORs in G9a/GLP dKO used to make RNA probes for FISH below. (**B**) 2-color FISH with Olfr231 probe in red and 10 other ORs in green including the 4 next-most highly expressed ORs in dKO (Olfr878, −1339, −464, −1361), 4 other highly upregulated ORs (Olfr446, −419, −433, −420) and 2 control probes that are readily detected in non-mutant E18.5 MOE (OIfr686, −556). Left is control, right is dKO. DAPI is removed from bottom panels. (**C**) Magnified view of inset as shown in (b) to highlight red/green coexpressing OSNs (arrowheads). Count totals for dKO are coexpressing cells: 49; Olfr231+ cells: 698; Olfr878 pool+: 350. Totals for control are: coexpressing cells: 0, Olfr231+: 4, Olfr878 pool+: 81.

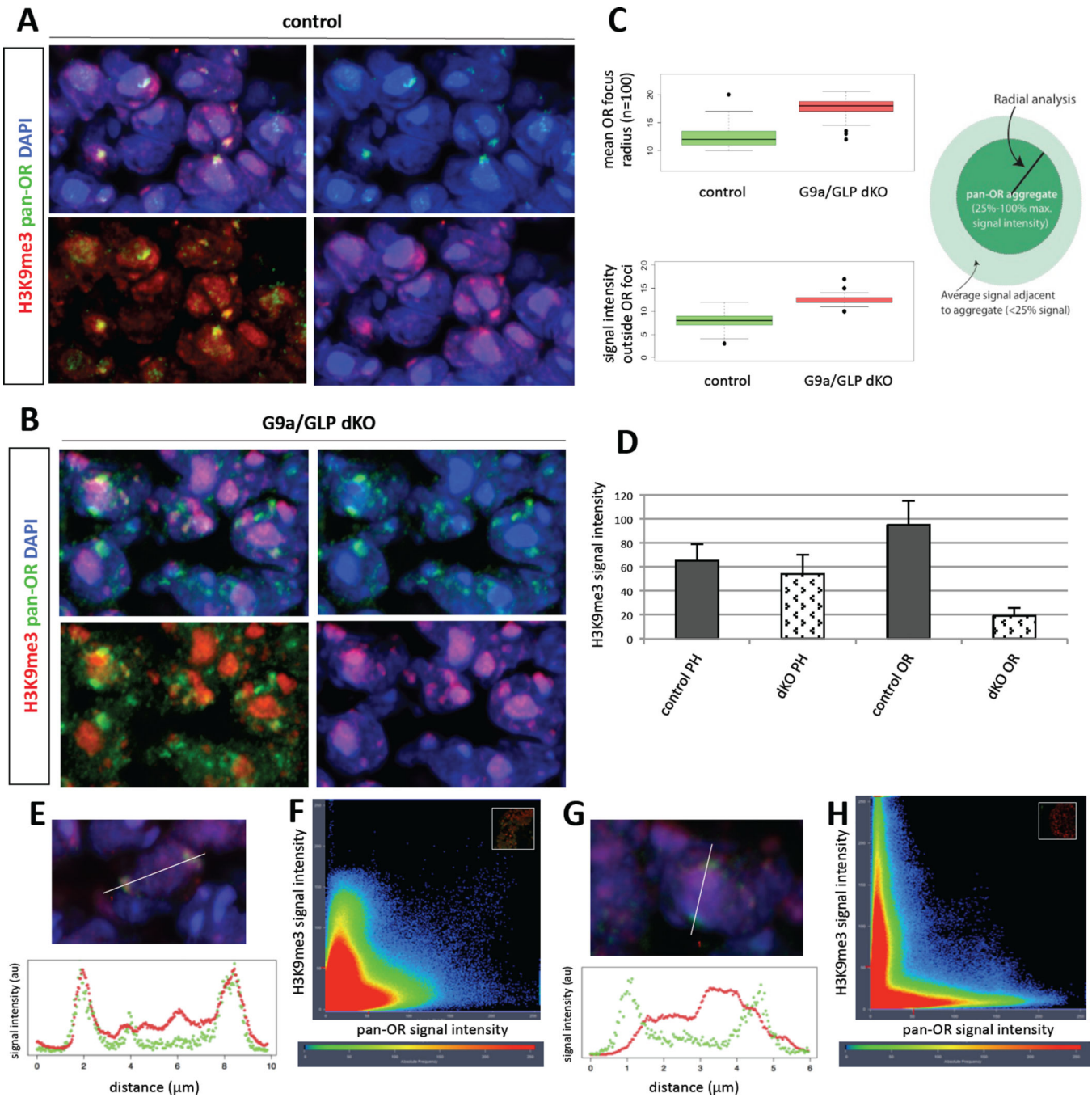

Figure 3. Heterochromatin is reduced at OR clusters in G9a/GLP dKO

(A and B) DNA FISH and immunofluoresence for OR gene cluster DNA (green; "pan-OR") and H3K9me3 (red) in MOE cryosections at E18.5 of control and G9a/GLP dKO, respectively. Upper left: merged image; upper right: pan-OR with DAPI; lower left: pan-OR with H3K9me3; lower right: H3K9me3 with DAPI. (C) Summary of measurements from pan-OR aggregate radial analysis (top) and peripheral signal quantification (bottom) (n=100 pan-OR foci for both). Cartoon depicts source of measurements for these analyses, whereby pan-OR aggregates were defined as the area containing signal between 25–100% maximum

intensity. (**D**) H3K9me3 signal intensity in two different regions of the nucleus illustrate a specific loss of H3K9me3 from OR gene foci in the dKO. PH: pericentromeric heterochromatin; OR: olfactory receptor gene aggregates. Error bars are standard deviation from the mean (for both genotypes: n_{PH}=50; n_{OR}=150). (**E and G**) Image of pan-OR and H3K9me3 in control and dKO, respectively, with reference line used for signal quantification (white, top panel); intensity plot corresponding to pixels intersecting reference line (bottom panel). (**F and H**) Pixel intensity plot for entire image plane (inset) (control and dKO, respectively). H3K9me3 intensity is plotted along y-axis; pan-OR is plotted on x-axis. Hotter colors correspond to greater frequency of occurrence. For **C, D, E, and G**, morphologically identified OSNs were used for measurements whereas **F** and **H** are quantifications of entire fields of cells in an MOE section.

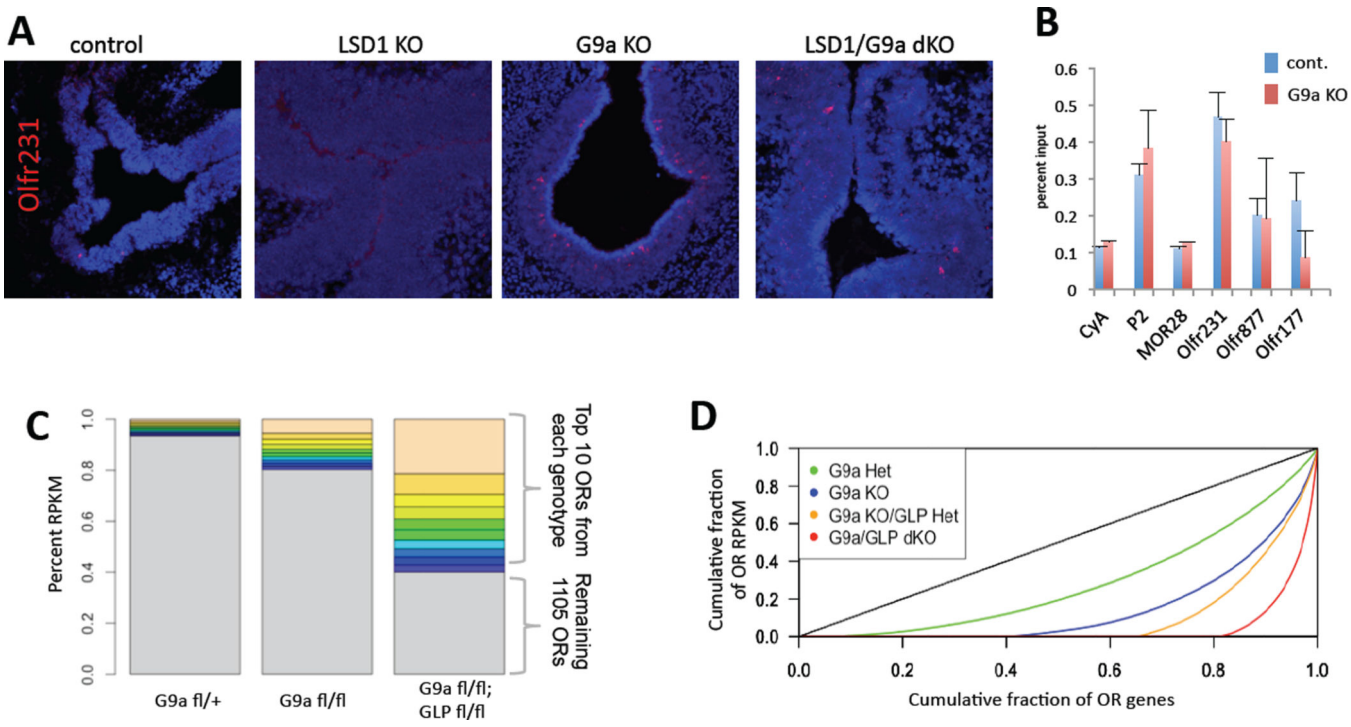

Figure 4. Reduction of H3K9me3 at OR genes allows LSD1-independent OR activation

(**A**) Olfr231 ISH in control (Cre-) MOE (leftmost) (average ~2 Olfr231+ cells per section n=20 sections) compared with (from left to right) LSD1 KO (average 0 Olfr231+ cells per section n=20), G9a KO (average ~38 Olfr231+ cells per section n=20 sections), and LSD1/G9a dKO (average ~4 Olfr231+ cells per section n=20) (for GLP KO: see Fig. S4). (**B**) 8-oxoguanosine DNA immunoprecipitation in G9a heterozygote (cont.) and G9a KO MOE at E18.5. Values represent the mean of technical duplicates; error bars are mean +/−SEM. (**C**) Percentage of total OR RPKM that the top ten most highly expressed ORs represent for each genotype as shown (all are Foxg1-Cre+, each color corresponds only to rank, not Olfr gene identity). Flox is abbreviated “fl”. (**D**) Lorenz curve depicting OR expression across all OR genes in the G9a-GLP dosage series (if all OR genes express at equal levels, Gini=0 and curve is perfect diagonal; see Fig. S2C–D). Curve depicts cumulative fraction of OR expression as a function of cumulative OR genes detected. (“Het”: flox/+; “KO”: flox/flox.)